Heliyon 10 (2024) e40642

Contents lists available at ScienceDirect

Heliyon

journal homepage: www.cell.com/heliyon

Research article

Optimizing acute chest pain diagnosis: Efficacy of 64-channel multi-slice CT with Snap-Shot Freeze technique in Triple-Rule-out CT angiography

Jie Feng [a,b,1], Jiale Zeng [a,1], Qiye Xu [a,1], Jiatian Lu [a], Yanru Pei [a], Xiang Zhang [a,**], Ming Gao [a,*]

[a] Department of Radiology, Sun Yat-Sen Memorial Hospital, Sun Yat-Sen University, No. 107 Yanjiang Road West, Guangzhou, 510120, China
[b] Xinxiang Medical University, Xinxiang, 453003, Henan, China

ARTICLE INFO

Keywords:
Acute chest pain (ACP)
Triple-Rule-out (TRO)
Computed tomography angiography (CTA)
64-Channel multi-slice CT (MSCT)
Snap-Shot Freeze (SSF)
Contrast medium (CM)
Image quality
Radiation dose

ABSTRACT

Objective: This study evaluates the efficacy of Snap-Shot Freeze (SSF) technology combined with optimized contrast medium (CM) injection protocols in Triple-Rule-Out (TRO) computed tomography angiography (CTA) using 64-channel multi-slice CT (MSCT) for diagnosing acute chest pain (ACP).

Materials and methods: A total of 111 patients presenting with ACP were enrolled and divided into two groups: Group 1 (23 patients) underwent TRO CTA using 64-channel MSCT with SSF technology, while the control group (88 patients) which was further divided into three cohorts underwent specific site CTA scans. Quantitative metrics such as CT values, standard deviation (SD), signal-to-noise ratio (SNR), and contrast-to-noise ratio (CNR) were calculated for pulmonary artery, coronary arteries, and aortic imaging. Demographic characteristics, image qualification rate and disease diagnosis rate of groups 1–4 were also evaluated. Qualitative evaluations were based on a 5-point scoring system assessing overall image quality, vessel clarity, and artifact presence. Radiation doses were measured in terms of CT dose index volume (CTDIvol), dose length product (DLP), and effective dose (ED).

Results: The demographic characteristics of the patients showed no significant differences in age, BMI, or resting heart rate between Group 1 and the control group. The image qualification rate was 100 % for both groups, with excellent rates of 89.13 % in Group 1 and 85.67 % in the control group. No significant differences were found in average CT values, standard deviation (SD), signal-to-noise ratio (SNR), and contrast-to-noise ratio (CNR) between Group 1 and the control group for pulmonary artery (e.g., PT: 394.25 ± 124.19 vs 383.64 ± 115.72 HU, $p = 0.74$), coronary artery (e.g., AA: 483.71 ± 115.62 vs 493.95 ± 138.54 HU, $p = 0.79$), and aorta (e.g., AAo: 325.1 ± 99.39 vs 348.98 ± 74.23 HU, $p = 0.34$). Qualitative image quality scores and radiation doses were also comparable (e.g., ED: 28.36 ± 12.6 vs 29.97 ± 10.36 mSv, $p = 0.77$). Qualitative assessments also revealed comparable image quality scores between the two groups (4.5 ± 0.5 vs 4.3 ± 0.6). The total volume of iodinated CM was significantly reduced in Group 1 (66 mL vs 227 mL).

* Corresponding author.
** Corresponding author.
E-mail addresses: zhangx345@mail.sysu.edu.cn (X. Zhang), gaoming2@mail.sysu.edu.cn (M. Gao).
[1] Jie Feng, Jiale Zeng and Qiye Xu have contributed equally to this work.

https://doi.org/10.1016/j.heliyon.2024.e40642
Received 10 September 2024; Received in revised form 5 November 2024; Accepted 21 November 2024
Available online 22 November 2024

Conclusion: The use of 64-channel MSCT combined with SSF technology in TRO CTA provides noninferior high-quality imaging comparable to traditional specific site CTA, with the added benefits of reduced CM volume and shorter examination times. This approach is effective for the comprehensive evaluation of ACP in clinical practice.

1. Introduction

Acute chest pain (ACP) is a condition characterized by high morbidity, mortality, and misdiagnosis rates, typically presenting as sudden, severe precordial pain [1]. Chest pain can result from various diseases, affecting approximately 25 % of the population, with primary causes including acute coronary syndrome (ACS), pulmonary thromboembolism (PTE), and aortic dissection (AD) [2]. The clinical symptoms of these conditions are similar, making timely diagnosis challenging based on clinical symptoms, laboratory tests, and ultrasound examinations alone [3,4]. The golden time window for symptom-to-first medical contact (SMC) in ST-segment elevation myocardial infarction (STEMI) patients is 120 min from symptom onset, with an ideal SMC time of less than 30 min [5]. For STEMI patients undergoing percutaneous coronary intervention (PCI), the door-to-wire (DW) time is 90 min and any longer than this time increases mortality [6]. Thus, early identification and timely, effective treatment are crucial in managing ACP [7,8].

With the advancement of multi-slice computed tomography (MSCT), Triple-Rule-Out (TRO) computed tomography angiography (CTA) has been recognized for its ability to simultaneously visualize the pulmonary artery, aorta, and other thoracic and abdominal structures, and noninvasively evaluate the coronary arteries. TRO CTA has become a research focus in recent years [9]. Wide-area detector CT (e.g., 256-detector rows CT and 16 cm z-axis detector CT) and dual-source CT have been increasingly used in clinical practice, making the scanning process rapid, simple, safe, and effective [10–13]. However, these technologies are expensive and their high costs limit their widespread adoption in primary hospitals and small to medium-sized cities [14].

In 2018, the National Cardiovascular Imaging Quality Control Expert Working Group surveyed 155 hospitals across China, finding that the average number of CT scanners with detector widths greater than 64 rows was only 1.08 per tertiary hospital and 0.29 per secondary hospital [15]. This indicates that about 70.55 % of CT devices in China have detector widths of 64 rows or less. Additionally, the application rates of coronary CTA, pulmonary CTA, and aortic CTA in secondary and tertiary hospitals were 64.5 % (91.9 % in tertiary hospitals, 46.2 % in secondary hospitals), 64.3 % (88.7 % in tertiary hospitals, 46.6 % in secondary hospitals), and 67.5 % (92.5 % in tertiary hospitals, 49.3 % in secondary hospitals), respectively [15].

Low-channel CT equipment often has insufficient temporal resolution, making it challenging to obtain high-quality TRO CTA images [16]. Scanning the three sites separately prolongs diagnosis time and increases the risk of renal injury due to multiple injections of iodinated contrast medium (CM) [17]. Snap-Shot Freeze (SSF) is a novel artifact correction algorithm in GE's 3rd generation CT equipment, compensating for coronary artery motion artifacts by using adjacent cardiac cycle image data [18]. This technology tracks the three-dimensional (3D) motion trajectory, speed, and direction of each coronary artery, providing motion-freezing and artifact correction at the 3D image level, thus enhancing image quality and diagnostic accuracy, especially in patients with high heart rates.

This study aims to analyze the application of SSF combined with contrast medium injection optimization in TRO CTA using 64-channel CT equipment.

2. Materials and methods

2.1. General information

The inclusion criteria for this study required patients to have no contraindications to CT scanning or related medications, such as oral beta-blockers or sublingual nitroglycerin, with informed consent obtained. Patients had to present with acute chest pain and have a high suspicion of ACS, PTE, AD based on physical examination or laboratory tests, without other causes of acute chest pain ruled out. Exclusion criteria included failure to complete CT scan with the study parameters, severe cardiac insufficiency or arrhythmias (e.g., atrial fibrillation or frequent premature beats), severe renal insufficiency or abnormal liver function, recent barium meal, allergy to iodinated contrast medium (CM), and being under 18 years of age or pregnant.

A total of 23 patients who underwent TRO CTA in our hospital from July 2020 to March 2022 were retrospectively included in the Group 1 (Group 1), comprising 12 males and 11 females, aged 24–75 years, with an average age of 51.83 ± 13.03 years and a body mass index (BMI) of 23.17 ± 2.95 kg/m^2. Simultaneously, 88 patients who underwent specific independent scans based on clinical manifestations and physical examination purposes formed the control group, including 49 males and 39 females, aged 24–87 years, with an average age of 60.21 ± 14.03 years and an average BMI of 22.65 ± 3.33 kg/m^2. The control group:

Group 2: 39 patients with pulmonary artery CTA (17 males and 22 females, aged 32–77 years, average age 58.08 ± 11.61 years, average BMI 22.67 ± 3.42 kg/m^2),

Group 3: 23 patients with coronary artery CTA (14 males and 9 females, aged 32–75 years, average age 56.65 ± 13.17 years, average BMI 23.66 ± 1.86 kg/m^2),

Group 4: 26 patients with aortic CTA (18 males and 8 females, aged 39–79 years, average age 56.65 ± 10.78 years, average BMI 21.74 ± 3.98 kg/m^2).

This retrospective study was approved by the hospital's ethics committee prior to initiation and was conducted in accordance with the Declaration of Helsinki. It was registered with the Chinese Clinical Trial Registry (Registration number: ChiCTR2200065068). The

study included patients who met the inclusion criteria and were scheduled for TRO CTA during the study period. A flowchart of the study enrollment is shown in Fig. 1.

2.2. Equipment and instruments

This study utilized a GE Discovery 750HD 64-channel spiral CT scanner, with image post-processing conducted on an Advanced Workstation 4.7 (AW 4.7). For the Group 1, a CT double-cylinder high-pressure syringe was employed, specifically the CT-200/200_Mark high-pressure syringe (Shenyang MasTech Medical Device Co., Ltd.). The contrast medium used was iopamidol injection (37 g of iodine per 100 mL), provided by Shanghai Bracco Sine Pharmaceutical Corp. Ltd. (Approval No. H20053388).

2.3. CT image acquisition

Comprehensive nursing intervention measures were implemented for all patients. Patients' heart rates were measured before scanning. For those with a heart rate (HR) greater than 80 beats per minute (BPM) and no contraindications to relevant drugs, HR control was achieved using the beta-blocker metoprolol as needed [19]. Additionally, sublingual administration of 0.8 mg nitroglycerin 3–5 min before scanning was used to improve the visualization of small lesions and enhance the diagnostic accuracy of Triple-Rule-Out CTA in evaluating the diameter and number of small artery segments, generally without causing serious adverse reactions or systemic physiological changes [20]. Operators were required to perform breath-holding training for all patients preparing for scanning, remove metal objects from their body surface, and clean the skin of their chest area. Electrocardiogram (ECG)-gated electrodes were attached to the patients and connected to the control device, with continuous monitoring of the patients' HR during breath-holding.

2.4. Group 1

Patients in the Group 1 were positioned supine, with an ECG gating device attached [21]. A cine segment scan was performed from below the tracheal bifurcation to below the heart using the parameters detailed in Table 1. Initially, 10 mL of iodine CM and 10 mL of

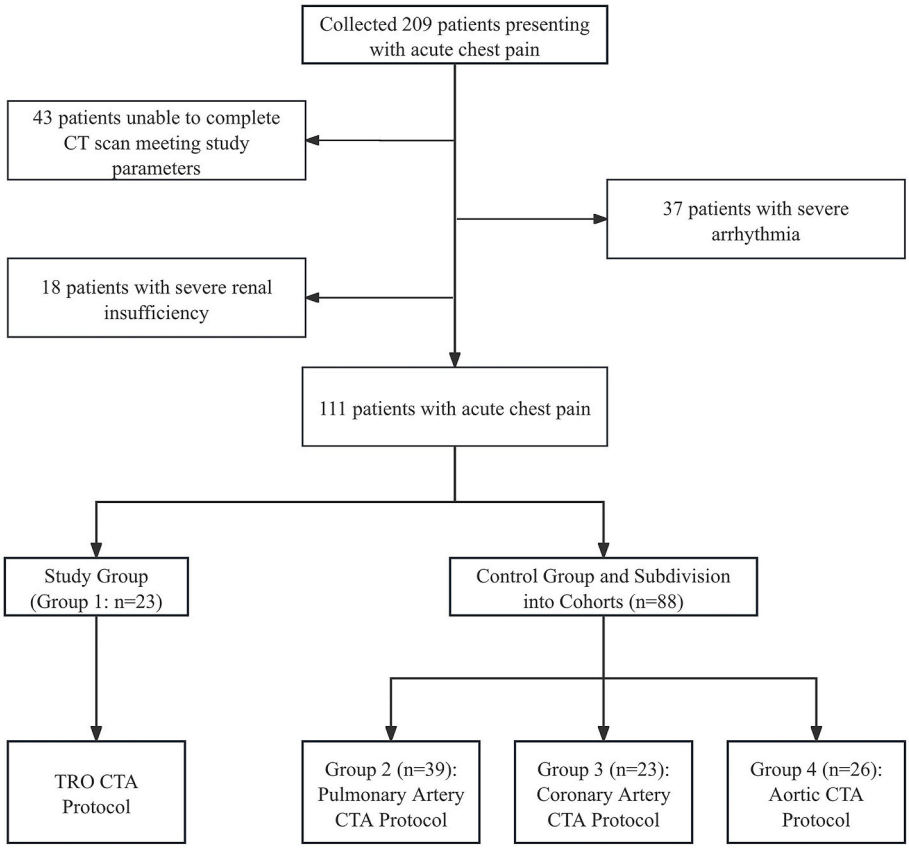

Fig. 1. Flowchart of the study enrollment.
Note.—TRO: Triple-Rule-Out; CTA: Computed Tomography Angiography.

saline were injected into the right elbow vein at a rate of 4 mL/s due to the use of an ultra-low dose contrast agent bolus injection for pre-injection [22]. Real-time changes in contrast concentration were monitored in the pulmonary artery (PA) and aortic root (AR) until the density in the AR decreased, indicating that the iodine contrast had passed its peak concentration. This observation allowed for the precise calculation of the peak transit times of the iodine contrast through the PA and AR by examining the time-density curves for contrast attenuation [23].

For the TRO CTA scan, an 18G intravenous (IV) trocar was used for a three-phase bolus injection: 40 mL of iodine CM at 5.0 mL/s, followed by 35 mL of a 3:1 mixture of iodine CM and saline at 3 mL/s, and finally 30 mL of saline at 5 mL/s, totaling 66 mL of iodinated contrast and 38 mL of saline over 26 s. The operator utilized time-density curves to calculate the delayed scanning time, using the formula:

$$T_{coronary} = T_{AR} + 10\text{s} - (T_{PA} + \text{PA scan time}), \quad (1)$$

where T_{PA} and T_{AR} is the peak iodine concentration time in the PA and AR, and $T_{coronary}$ is the delay time that needs to be calculated to scan coronary CTA. The aorta was scanned immediately after the coronary phase. CT parameters and coronary phase pitch were measured by ECG, employing reconstruction methods such as Snap-Shot Segment, Temporal Enhance, and intelligent tube current control. The PA was scanned from the thoracic inlet to the costophrenic angle, the coronary arteries from 1 cm below the tracheal bifurcation to below the diaphragmatic surface of the heart, and the aorta from the thoracic entrance to the inferior pubic symphysis. Detailed parameters are provided in Table 1.

2.5. Control groups

Patients in the control groups were positioned similarly to those in the Group 1. Group 2 underwent scanning from the thoracic entrance to the costophrenic angle, Group 3 from 1 cm below the tracheal bifurcation to below the diaphragmatic surface of the heart, and Group 4 from the thoracic entrance to the lower margin of the symphysis pubis. An 18G trocar was used for puncturing the right antecubital vein, and a CT syringe facilitated the injection. In Groups 2–4, 50, 60, and 80 mL of iodine CM were injected at 5.0 mL/s during the first stage of CTA scanning, followed by 20 mL of normal saline at 5.0 mL/s in the second stage, resulting in a total injection volume of 70–100 mL and an injection time of 12–20 s. The specific parameters for these groups are detailed in Table 2.

2.6. CT image reconstruction and evaluation

For image reconstruction in Group 1, the study employed GE Healthcare's ASIR algorithm with a strength of 70 %. The AW 4.7 was used to analyze the PA, coronary artery (CA), aorta, and major tissues utilizing SSF technology. Various image processing techniques, including Volume Rendering (VR), Maximum Intensity Projection (MIP), Curved Planar Reconstruction (CPR), and Multiplanar Reformation (MPR), were applied to generate 3D images for further analysis.

Axial images were analyzed by placing regions of interest (ROI) in the main pulmonary artery trunk (PT), left/right pulmonary artery trunk (LPT/RPT), the right erector spinae at the bifurcation of the trachea (RESBT), left main coronary artery (LMA), proximal left anterior descending Artery (LAD-p), proximal left circumflex artery (LCX-p), proximal right coronary artery (RCA-p), pericardial fat (PF), lateral wall of the left ventricle (LVLW), ascending aortic orifice (AAo), ascending aorta (AA), descending aorta (DAo), aortic arch (AAr), the abdominal aorta at the level of the first hilum hepatis (AA_FHH), and the right erector spinae muscle at the measurement level. ROIs were consistently placed to avoid calcification, plaque, and lesions. Data were measured three times on consecutive axial images and averaged. The average CT value and SD were recorded. The SNR and CNR were then calculated using the

Table 1
Scanning parameters of group 1.

Scan Conditions	Calcification Score	Pulmonary Arterial Phase	Coronary Phase	Thoracoabdominal Aortic Phase
Tube voltage (KV)	120	120	120	120
Tube current (mA)	Manual mA 300	Smart mA 150–500	ECG modulated mA 275-695	Smart mA 150–500
Index of noise	–	8.5	–	8.5
Scan mode	Cine	Helical	Cardiac	Helical
Speed of rotation	0.35	0.4	0.35	0.4
Detector width (mm)	40	40	40	40
Pitch	2.5 16i	1.531:1	Smart	1.531:1
FOV	Large Body	Large Body	Cardiac Large	Large Body
matrix	512 × 512	512 × 512	512 × 512	512 × 512
Scan slice thickness (mm)	2.5	5	2.5	5
Preset ASiR (%)	50	50	50	50
Reconstruction layer thickness (mm)	2.5	1.25	0.625	1.25
Rebuild layer spacing (mm)	40	1	0.625	1
Reconstruction of ASiR (%)	50	70	50	70
Reconstruction algorithm	Stnd	Soft	Stnd/Detail	Soft
Rebuild window width	400	350	800	350
Rebuild window levels	40	50	100	50

Note.—Abbreviations KV: kilovoltage; mA: milliampere; FOV: Field of View; mm: millimeter; ASiR: Adaptive Statistical Iterative Reconstruction.

Table 2
Scanning parameters of control group.

Scan Conditions	Group 2	Group 3 for Calcification score	Group 3	Group 4
Tube voltage (KV)	120	120	120	120
Tube current (mA)	Smart mA 150–350	Manual mA 300	ECG modulated mA 250-550	Smart mA 150–350
Noise index	11.57	–	–	11.57
Scan mode	Helical	Cine	Cardiac	Helical
Speed of rotation	0.5	0.35	0.35	0.5
Detector width (mm)	40	40	40	40
Pitch	1.375:1.	2.5 16i	Smart	1.375:1
FOV	Large Body	Large Body	Cardiac Large	Large Body
matrix	512 x 512	512 x 512	512 × 512	512 × 512
Scan slice thickness (mm)	5	2.5	2.5	5
Preset ASiR (%)	50	50	50	50
Reconstruction layer thickness (mm)	1.25	2.5	0.625	1.25
Rebuild layer spacing (mm)	1	40	0.625	1
Reconstruction of ASiR (%)	50	50	50	50
Reconstruction algorithm	Soft	Stnd	Stnd/Detail	Soft
Rebuild window width	350	400	800	350
Rebuild window levels	50	40	100	50

Note.—Abbreviations KV: kilovoltage; mA: milliampere; FOV: Field of View; mm: millimeter; ASiR: Adaptive Statistical Iterative Reconstruction.

following formulas [24,25]:

$$SNR = \frac{P_{signal}}{Noise\ SD}, \tag{2}$$

$$CNR = \frac{P_{signal} - P_{background}}{Noise\ SD}, \tag{3}$$

where P_{signal} is the average CT number of the signal region, $P_{background}$ is the average CT number of the background region around the signal, and *Noise SD* is the standard deviation (SD) of the background region. Images were evaluated by two radiologists with more than five years of experience, and disagreements were resolved by consensus.

Qualitative assessments metrics was scored based on pulmonary circulation imaging, the American Heart Association's modified 15-segment classification [26], aortic/branch imaging [27,28], and a 5-point scoring system as follows [29–32]: 5 = Excellent quality, clear vessels, no artifacts, 4 = Good quality, slightly blurred edges, no major artifacts, 3 = Fair quality, blurred edges with minimal impact on diagnosis, 2 = Poor quality, motion artifacts and disconnected vessels, 1 = Very poor quality, severe artifacts.

Overall image quality was also evaluated.

① Overall Image Quality Score: 5 = Clear image, no noise, 4 = Clear image, minimal noise, 3 = Diagnosable image, acceptable noise, 2 = Blurred image, difficult diagnosis, noticeable noise, 1 = Unclear image, difficult diagnosis, significant noise.
② Image Noise Score: 5 = Almost no noise, smooth image, 4 = Small noise, smooth image, 3 = Minimal noise, light grain feeling, 2 = Noticeable noise, strong graininess, difficult diagnosis, 1 = Significant noise, strong grain, affects structure display and recognition.

Qualified rate are defined as qualitative evaluation score 3 points or more, excellent rate is defined as qualitative evaluation score equal to 5.

2.7. Radiation dose calculation

The CT dose index volume (CTDIvol, unit: mGy), dose length product (DLP, unit: mGy * cm), and were recorded by the system after each scan. The effective dose (ED, unit: mSv) was calculated using the formula [33]:

$$ED = k \times DLP, \tag{4}$$

where the k value is:
k = 0.014 (mSv * $mGy^{-1}{\cdot}cm^{-1}$) for pulmonary artery CTA [34],
k = 0.026 (mSv * $mGy^{-1}{\cdot}cm^{-1}$) for calcium score and coronary artery CTA [35,36],
k = 0.0145 (mSv * $mGy^{-1}{\cdot}cm^{-1}$) for the average value of thoracoabdominal aorta CTA [37].

2.8. Statistical analysis

Statistical analyses were conducted using SPSS v. 24.0 (IBM Corp., NY). The Shapiro-Wilk test assessed data normality. Normally distributed data were presented as mean ± SD, while non-normally distributed data were shown as median (quartiles). Categorical

data were expressed as frequency (percentage). For comparisons, a two-sample *t*-test was used for normally distributed data with equal variances, and a corrected *t*-test for unequal variances. The Mann-Whitney *U* test was applied for non-normally distributed data. One-way analysis of variance (ANOVA) was used for normally distributed data across multiple groups, and the Kruskal-Wallis H test for non-normally distributed data. Categorical data were analyzed with the χ^2 test. Image quality scores were compared using the Mann-Whitney *U* test for two groups and the Jonckheere-Terpstra test for multiple groups. Quantitative and qualitative evaluations were performed by at least two physicians, with inter-observer agreement assessed. The intraclass correlation coefficient (ICC) evaluated quantitative assessments, while the Kappa coefficient assessed qualitative ones, interpreted as: 0–0.20 (Poor), 0.21–0.40 (Fair), 0.41–0.60 (Moderate), 0.61–0.80 (Substantial), 0.81–1.00 (Almost perfect). The Hodges-Lehmann estimator provided the median difference (95 % confidence intervals (CI)) based on the Mann-Whitney *U* test, with a two-tailed P-value <0.05 indicating statistical significance.

3. Results

3.1. Patient characteristics

After applying the exclusion criteria, the study population consisted of 111 patients, all of whom successfully completed the examination. A total of 111 patients with ACP were diagnosed by CT images, including 6 cases of pulmonary embolism (26.09 %), 5 cases of aortic dissection (21.73 %), 1 case of ascending aortic aneurysm (4.35 %), 9 cases of coronary artery stenosis (39.13 %), including 1 case of myocardial infarction (4.35 %) after stent implantation and aortic valve catheterization. Pulmonary embolism was found in 24 patients (61.54 %) in group 2. In group 3, 13 patients (56.52 %) had coronary artery stenosis and 6 patients (26.09 %) had myocardial bridge. In group 4, there were 4 cases of aneurysm (15.38 %), 2 cases of aortic intramural hematoma (7.69 %) and 1 case of aortic coarctation (3.84 %).

In addition, the age of enrolled patients ranged from 24 to 79 years, with an average age of 56.15 ± 12.12 years. The average BMI was 22.76 ± 3.25 kg/㎡. Among the participants, 54.95 % were male (61 of 111) and 45.05 % were female (50 of 111). Table 3 summarizes the characteristics of the patients.

There were no significant differences in age, BMI, or resting HR between the Group 1 and the control group (F = 1.35, 1.61, 0.19; P = 0.26, 0.19, 0.90, respectively). Additionally, there was no significant difference in the male-to-female ratio ($\chi^2 = 4.53$, P = 0.21).

3.2. Quantitative analysis of CT images

3.2.1. Quantitative analysis and comparison of pulmonary CTA between group 1 and group 2

Quantitative analysis revealed no significant difference in the average CT values (measured in Hounsfield units, HU) of the PT, LPT, RPT, and RESBT between Group 1 and Group 2. The values were: PT, 10.61 (95 % CI: −51.91 to 73.14, p = 0.74); LPT, 1.68 (95 % CI: −52.99 to 56.32, p = 0.95); RPT, −10.92 (95 % CI: −67.58 to 45.73, p = 0.70); and RESBT, 2.92 (95 % CI: −5.37 to 11.21, p = 0.40) (Table 4, Fig. 2A).

Similarly, there were no significant differences in the SD of CT values: PT, 1.00 (95 % CI: −1.09 to 3.07, p = 0.34); LPT, −0.22 (95 % CI: −2.99 to 2.56, p = 0.88); RPT, −0.34 (95 % CI: −3.51 to 2.83, p = 0.83) (Fig. 2B).

SNR values also showed no significant differences: PT, −1.14 (95 % CI: −6.36 to 4.09, p = 0.67); LPT0.92 (95 % CI: −3.82 to 5.67, p = 0.69); RPT, −0.76 (95 % CI: −4.25 to 2.73, p = 0.67) (Fig. 2C).

Furthermore, CNR values were not significantly different: PT, 1.36 (95 % CI: −4.11 to 6.82, p = 0.64); LPT, 0.64 (95 % CI: −4.03 to 5.30, p = 0.78); RPT, 1.05 (95 % CI: −4.53 to 2.44, p = 0.56) (Fig. 2D).

In conclusion, the quantitative assessment of PA image quality using CT values, SD, SNR and CNR revealed no statistically significant differences between traditional PA CTA and TRO CTA. This finding suggests that TRO CTA is as effective as traditional PA CTA in terms of quantitative image evaluation metrics.

3.2.2. Quantitative assessment and comparison of coronary CTA between group 1 and group 3

Quantitative analysis revealed no significant differences in the average CT values of the AA, LMA, LAD-p, LCX-p, RCA-p, PF, and LVLW between Group 1 and Group 3. The specific values were as follows: AA, −10.23 (95 % CI: −86.06 to 65.60, p = 0.79); LMA, −16.11 (95 % CI: −99.54 to 67.32, p = 0.70); LAD-p, −48.88 (95 % CI: −151.25 to 53.37, p = 0.34); LCX-p, 7.14 (95 % CI: −81.31 to

Table 3
Comparison of Patient characteristics between the group 1 and the control group.

	Group 1	Group 2	Group 3	Group 4	Value of test	*p* value
Age (y)	51.83 ± 13.03	58.08.9 ± 11.61	56.65 ± 13.17	56.65 ± 10.78	1.35 [F]	0.26
Gender						
No. of men (%)	12(52.17)	17(58.62)	14(60.87)	18(69,23)	4.53 [H]	0.21
No. of women (%)	11(47.83)	22(41.38)	9(39.13)	8(30.77)		
BMI (kg/㎡)	23.17 ± 2.95	22.67 ± 3.42	23.66 ± 1.86	21.74 ± 3.98	1.61 [F]	0.19
Resting heart rate	67.83 ± 10.54	67.10 ± 10.40	66.57 ± 9.92	67.55 ± 14.61	0.19 [F]	0.90

Note.—Values are means ± standard deviations; BMI: Body Mass Index; n (%); [F]: F value of ANOVA; [H]: H value of Kruslal-Wallis test; *: Compared with group 1, $p < 0.05$.

Table 4
CT values (HU) of pulmonary artery CTA in group 1 and group 2.

	PT	LPT	RPT	RESBT
Group 1	394.25 ± 124.19	353.04 ± 110.15	353.16 ± 114.38	58.00 ± 12.75
Group 2	383.64 ± 115.72	351.38 ± 100.16	364.08 ± 103.68	60.65 ± 11.22
T value	0.34	0.06	−0.37	−0.85
P value	0.74	0.95	0.70	0.40

Note.—Values are means ± standard deviations; PT: Pulmonary Artery Trunk; LPT: Left Pulmonary Artery Trunk; RPT: Right Pulmonary Artery Trunk; RESBT: Right Erector Spinae at the Bifurcation of the Trachea; *: Compared with group 1, p < 0.05.

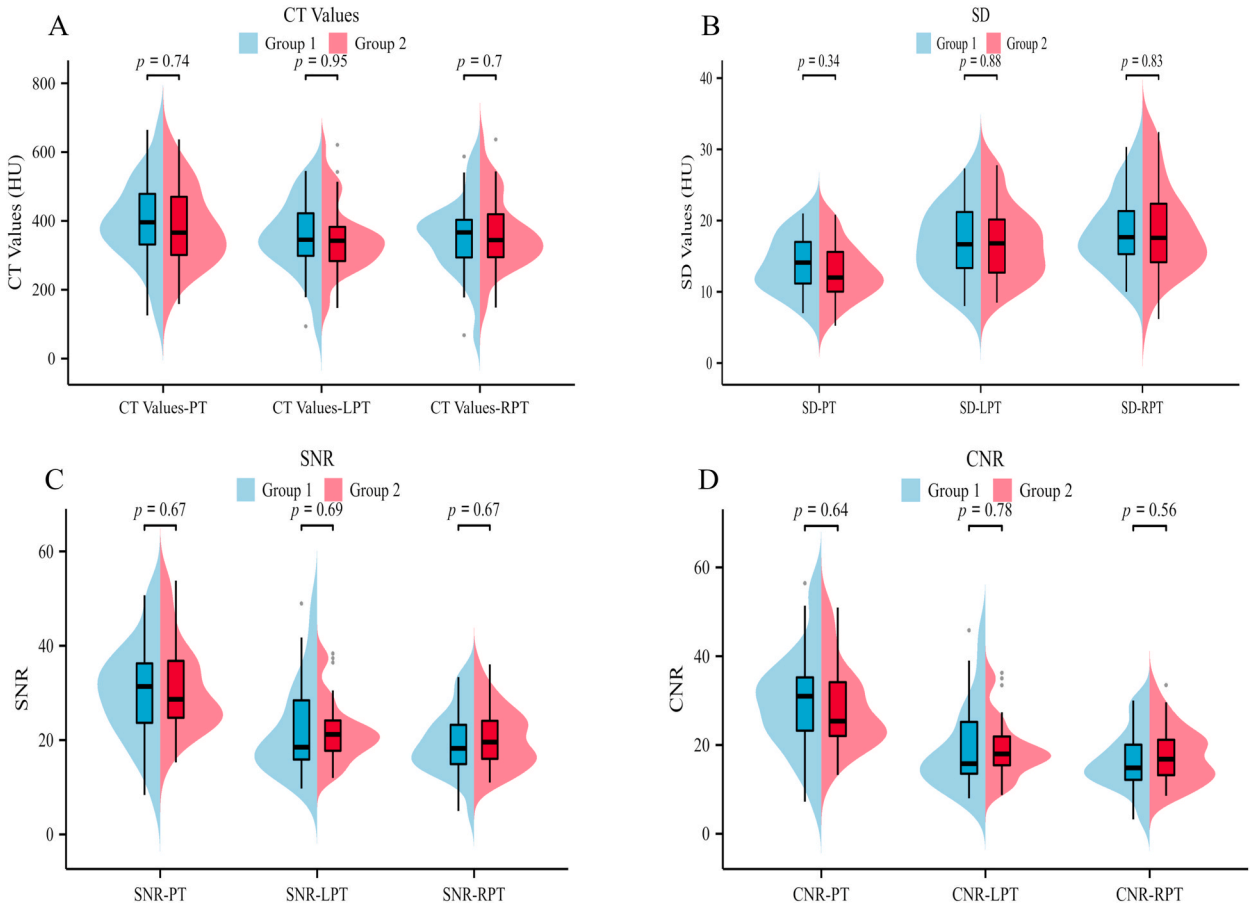

Fig. 2. Comparative Analysis of Quantitative Assessment Metrics for Group 1 and Group 2. **A-D:** Statistical representations of CT values, standard deviation (SD), signal-to-noise ratio (SNR), and contrast-to-noise ratio (CNR) for the pulmonary trunk (PT), left pulmonary trunk (LPT), and right pulmonary trunk (RPT). *: Compared with group 1, $p < 0.05$.

Table 5
CT values (HU) of coronary CTA in group 1 and group 3.

	AA	LMA	LAD-p	LCX-p	RCA-p	PF	LVLW
Group 1	483.71 ± 115.62	465.59 ± 134.74	441.36 ± 138.57	446.2 ± 145.73	426.18 ± 106.63	−97.15 ± 16.21	98.08 ± 22.25
Group 3	493.95 ± 138.54	481.70 ± 145.82	490.24 ± 199.99	439.06 ± 151.90	467.19 ± 157.96	−99.97 ± 23.86	97.90 ± 27.33
T value	−0.27	−0.39	−0.96	0.16	−1.03	0.47	0.03
P value	0.79	0.70	0.34	0.87	0.31	0.64	0.98

Note.—Values are mean ± standard deviations; AA: Ascending Aorta; LMA: Left Main Coronary Artery; LAD-p: Proximal Left Anterior Descending Artery; LCX-p: Proximal Left Circumflex Artery; RCA-p: Proximal Right Coronary Artery; PF: Pericardial Fat; LVLW: Left Ventricular Lateral Wall; *: Compared with group 1, $p < 0.05$.

95.61, p = 0.87); RCA-p, −41.01 (95 % CI: −121.41 to 39.40, p = 0.31); PF, 2.82 (95 % CI: −9.31 to 14.94, p = 0.64); and LVLW, 0.18 (95 % CI: −14.63 to 14.99, p = 0.98) (Table 5 and Fig. 3A).

There were also no significant differences in the SD values for AA, −2.85 (95 % CI: −6.18 to 0.48, p = 0.09); LMA, −0.11 (95 % CI: −6.36 to 4.03, p = 0.65); LAD-p, −7.23 (95 % CI: −16.05 to 1.59, p = 0.14); LCX-p, 10.61 (95 % CI: −51.91 to 73.14, p = 0.92); RCA-p, −00.07 (95 % CI: -7.42 to 7.28, p = 0.68); PF, −1.18 (95 % CI: −4.90 to 2.54, p = 0.53); and LVLW, −2.25 (95 % CI: −6.46 to 1.96, p = 0.29) (Fig. 3B–C).

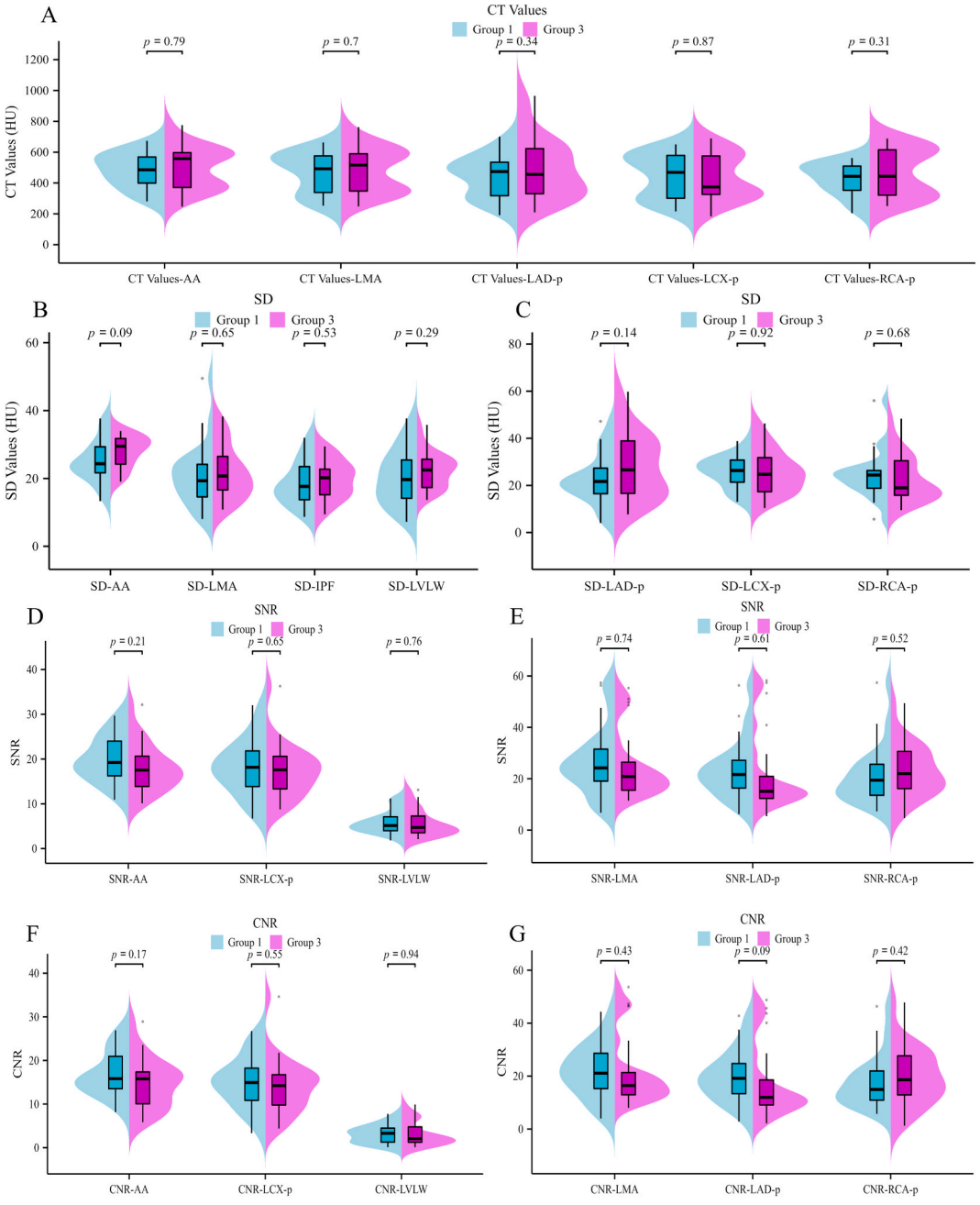

Fig. 3. Comparative Analysis of Quantitative Assessment Metrics for Group 1 and Group 3. **A:** Statistical plots of CT values for the ascending aorta (AA), left main artery (LMA), proximal left anterior descending artery (LAD-p), proximal left circumflex artery (LCX-p), and proximal right coronary artery (RCA-p). **B:** Statistical plots of standard deviation (SD) for the AA, LMA, pulmonary trunk (PT), and left ventricular lateral wall myocardium (LVLM). **C:** Statistical plots of SD for the LAD-p, LCX-p, and RCA-p. **D:** Statistical plots of signal-to-noise ratio (SNR) for the AA, LCX-p, and LVLM. **E:** Statistical plots of SNR for the LMA, LAD-p, and RCA-p. **F:** Statistical plots of contrast-to-noise ratio (CNR) for the AA, LCX-p, and LVLM. **G:** Statistical plots of CNR for the LMA, LAD-p, and RCA-p. *: Compared with group 1, $p < 0.05$.

The SNR values also showed no significant differences: AA, 1.99 (95 % CI: −1.17 to 5.15, p = 0.21); LMA, 2.61 (95 % CI: −6.41 to 11.63, p = 0.74); LAD-p, 1.61 (95 % CI: −8.87 to 12.09, p = 0.61); LCX-p, −0.62 (95 % CI: −5.53 to 4.29, p = 0.65); RCA-p, −2.07 (95 % CI: −8.54 to 4.40, p = 0.52); and LVLW, 0.25 (95 % CI: −1.41 to 1.90, p = 0.76) (Fig. 3D–E).

Similarly, the CNR values were not significantly different: AA, 2.28 (95 % CI: −1.02 to 5.58, p = 0.17); LMA, 2.90 (95 % CI: −6.00 to 11.80, p = 0.43);, LAD-p, 1.90 (95 % CI: −8.67 to 12.47, p = 0.09); LCX-p, −0.33 (95 % CI: −5.27 to 4.60, p = 0.55); RCA-p, −1.78 (95 % CI: −8.13 to 4.58, p = 0.42); and LVLW, −0.06 (95 % CI: −1.55 to 1.43, p = 0.94) (Fig. 3F–G).

In summary, the quantitative evaluation of coronary artery image quality using CT values, SD, SNR, and CNR showed no statistically significant discrepancies between conventional coronary CTA and TRO CTA. This result suggests that TRO CTA is equally efficacious as traditional coronary CTA in regard to quantitative image assessment metrics.

3.2.3. Quantitative assessment and comparison of aorta CTA between groups 1 and 4

Quantitative analysis revealed no significant differences in the average CT values of the ascending aorta orifice (AAo), descending aorta (DAo), aortic arch (AAr), and abdominal aorta at the level of the first hepatic hilum (AA_FHH) between Group 1 and Group 4. The specific values were as follows: AAo, −23.88 (95 % CI: −73.93 to 26.17, p = 0.34); DAo, −4.61 (95 % CI: −53.62 to 44.41, p = 0.85); AAr, −29.10 (95 % CI: −71.46 to 13.26, p = 0.17) and AA_FHH, 12.10 (95 % CI: −58.01 to 33.82, p = 0.60) (Table 6 and Fig. 4A).

There were also no significant differences in the SD values for AAo, −2.66 (95 % CI: −7,17 to 1.85, p = 0.25); DAo, −0.27 (95 % CI: −4.54 to 3.40, p = 0.90); AAr, 0.09 (95 % CI: −2.00 to 2.18, p = 0.93) and AA_FHH, 1.21 (95 % CI: −1.76 to 4.19, p = 0.42) (Fig. 4B).

The SNR values also showed no significant differences: AAo, 3.76 (95 % CI: −1.37 to 8.89, p = 0.15); DAo, 1.43 (95 % CI: −2.99 to 5.84, p = 0.52); AAr, −2.75 (95 % CI: −7.75 to 2.25, p = 0.27) and AA_FHH, −1.03 (95 % CI: −4.93 to 2.88, p = 0.61) (Fig. 4C).

Similarly, the CNR values were not significantly different: AAo, 3.53 (95 % CI: −1.65 to 5.58, p = 0.18); DAo, 1.20 (95 % CI: −3.22 to 5.61, p = 0.59); AAr, −2.98 (95 % CI: −8.01 to 2.06, p = 0.23) and AA_FHH, −1.91 (95 % CI: −5.70 to 1.88, p = 0.32) (Fig. 4D).

In conclusion, the quantitative evaluation of aortic image quality utilizing CT values, SD, SNR, and CNR demonstrated no statistically significant variances between conventional aortic CTA and TRO CTA. This observation suggests that TRO CTA is equally efficacious as traditional aortic CTA in relation to quantitative image assessment parameters.

3.2.4. Qualitative analysis and comparison of images in groups 1-4

The qualitative analysis method was employed to evaluate the image quality across groups 1–4, encompassing 888 vessels and 3547 segments. The results, as detailed in Table 7, indicate that the Kappa values for qualitative analysis scores of vessel levels, vessel segments, overall image quality, and noise perception ranged from 0.6 to 0.9, demonstrating good inter-observer agreement. Both the Mann-Whitney *U* test and Jonckheere-Terpstra test revealed no significant differences in qualitative analysis scores ($P > 0.05$), with a diagnostic rate of 100 %. Specifically:

For the PT, no significant difference was observed between Group 1 and Group 2, with 93.5 % of segments in Group 1 rated as 5 and 6.5 % as 4, compared to 93.6 % and 6.4 % in Group 2, respectively ($Z = -0.02$, $P = 0.98$). Similarly, for the Left LPT, 95.7 % of segments in Group 1 were rated as 5 and 4.3 % as 4, while in Group 2, 98.7 % were rated as 5 and 1.3 % as 4 ($Z = -1.86$, $P = 0.06$). For the RPT, 82.1 % of segments in Group 1 were rated as 5 and 17.9 % as 4, compared to 87.8 % and 12.2 % in Group 2 ($Z = -1.77$, $P = 0.08$).

In the LMA, 93.5 % of segments in Group 1 were rated as 5 and 6.5 % as 4, while in Group 3, 89.1 % were rated as 5 and 10.9 % as 4 ($Z = -0.74$, $P = 0.46$). For the LAD, 89.1 % of segments in Group 1 were rated as 5, 9.6 % as 4, and 1.3 % as 3, compared to 90.9 %, 6.1 %, and 3.0 % in Group 3 ($Z = -0.55$, $P = 0.59$). Additionally, for the LCX, 87.1 % of segments in Group 1 were rated as 5 and 12.9 % as 4, while in Group 3, 91.7 % were rated as 5, 4.8 % as 4, and 1.8 % as 3 ($Z = -1.46$, $P = 0.14$). For the RCA, 85.0 % of segments in Group 1 were rated as 5, 13.7 % as 4, and 1.3 % as 3, compared to 86.0 %, 13.2 %, and 1.1 % in Group 3 ($Z = -0.30$, $P = 0.76$).

For the aorta, Group 1 had 496 segments (98.0 %) rated as 5 and 10 segments (2.0 %) as 4, with a Kappa value of 0.80. Group 4 had 551 segments (96.3 %) rated as 5 and 21 segments (3.7 %) as 4, with a Kappa value of 0.85 ($Z = -1.67$, $P = 0.10$), indicating no significant difference.

The overall quality scores showed no significant difference among the four groups. Group 1 had 51 segments (55.4 %) rated as 5, 33 segments (35.9 %) as 4, and 8 segments (8.7 %) as 3, with a Kappa value of 0.81. Group 2 had 73 segments (46.8 %) rated as 5, 77 segments (49.4 %) as 4, and 3 segments (3.8 %) as 3, with a Kappa value of 0.88. Group 3 had 45 segments (48.9 %) rated as 5, 45 segments (48.9 %) as 4, and 2 segments (2.2 %) as 3, with a Kappa value of 0.88. Group 4 had 51 segments (49.0 %) rated as 5, 45 segments (43.3 %) as 4, and 8 segments (7.7 %) as 3, with a Kappa value of 0.87. The J value from the Jonckheere-Terpstra test was −3.51, and the P value was 0.60, indicating no significant difference.

Table 6
CT values (HU) of aortic CTA in group 1 and group 4.

	AAo	DAo	AAr	AA_FHH
Group 1	325.1 ± 99.39	318.25 ± 88.57	298.54 ± 70.89	295.52 ± 81.3
Group 4	348.98 ± 74.23	322.85 ± 81.96	327.63 ± 75.82	307.62 ± 78.31
T value	−0.96	0.19	−1.38	−0.53
P value	0.34	0.85	0.17	0.60

Note.—Values are means ± standard deviations; AAo: Ascending Aorta Orifice; DAo: Descending Aorta; AAr: Aortic Arch; AA_FHH: Abdominal Aorta at The Level of The First Hepatic Hilum; *: Compared with group 1, $p < 0.05$.

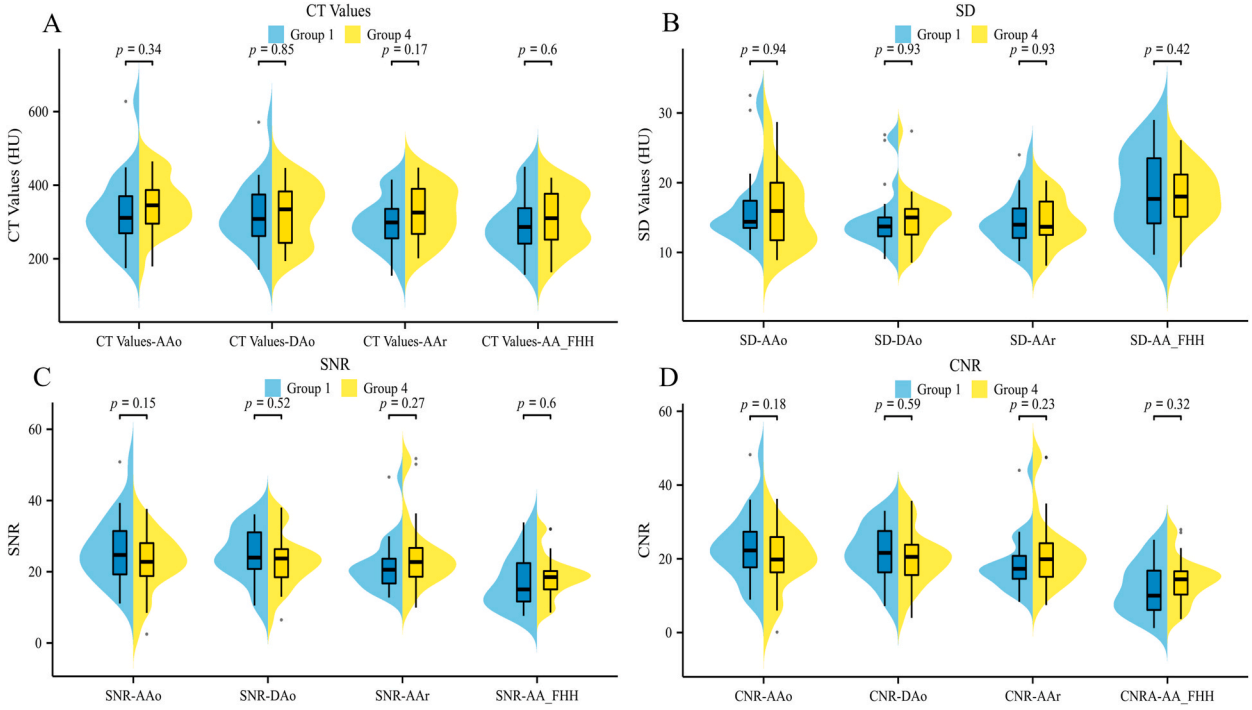

Fig. 4. Comparative Analysis of Quantitative Assessment Metrics for Group 1 and Group 4. **A-D:** Statistical plots of CT values, standard deviation (SD), signal-to-noise ratio (SNR), and contrast-to-noise ratio (CNR) for the ascending aorta orifice (AAo), descending aorta (DAo), aortic arch (AAr), and abdominal aorta at the level of the first hepatic hilum (AA_FHH). *: Compared with group 1, $p < 0.05$.

The noise scores also showed no significant difference among the four groups. Group 1 had 33 segments (71.7 %) rated as 4 and 13 segments (28.3 %) as 3, with a Kappa value of 0.83. Group 2 had 70 segments (89.7 %) rated as 4 and 8 segments (10.3 %) as 3, with a Kappa value of 0.72. Group 3 had 43 segments (93.5 %) rated as 4 and 3 segments (6.5 %) as 3, with a Kappa value of 0.65. Group 4 had 40 segments (76.9 %) rated as 4 and 12 segments (23.1 %) as 3, with a Kappa value of 0.79 (J = 0.66, P = 0.51), indicating no significant difference.

3.3. Analysis and comparison of radiation doses in groups 1-4

In this study, the comparison of radiation doses among the four patient groups revealed no statistically significant differences in terms of CTDIvol, DLP, and ED values (P > 0.05), as shown in Table 8. Specifically, for CTDIvol (mGy) values for the PA were 0.65 (95 % CI: −1.09 to 1.49, p = 0.76) between group 1 and group 2; for Coronary, −7.49 (95 % CI: −17.8 to 2.82, p = 0.15) between group 1 and group 3; and for Ao, −0.13 (95 % CI: −1.46 to 1.19, p = 0.84) between group 1 and group 4. In terms of DLP (mGy·cm) values for the PA were 27.87 (95 % CI: −23.21 to 78.96, p = 0.28) between group 1 and group 2; for Coronary, −86.78 (95 % CI: −247.63 to 74.07, p = 0.28) between group 1 and group 3; and for Ao, 17.85 (95 % CI: −103.22 to 138.92, p = 0.77) between group 1 and group 4. In terms of ED (mSv) values for the PA were 0.39 (95 % CI: −0.33 to 1.11, p = 0.28) between group 1 and group 2; for Coronary, −2.26 (95 % CI: −6.44 to 1.92, p = 0.28) between group 1 and group 3; and for Ao, 0.26 (95 % CI: −1.50 to 2.01, p = 0.77) between group 1 and group 4.

In summary, the analysis of radiation doses, including CTDIvol, DLP, and ED, among the four groups showed no significant differences, indicating that the use of 64-channel MSCT combined with the coronary SSF technique provides consistent radiation exposure levels across different patient groups.

4. Discussion

4.1. Significance of 64-channel MSCT for TRO CTA

This study included a total of 111 patients, with 23 in the Group 1 and 88 in the control group. The qualified rate in both groups was 100 % (qualitative evaluation score ≥3), and the excellent rate was 89.13 % in the Group 1 and 85.67 % in the control group (qualitative evaluation score = 5). These findings demonstrate that 64-channel MSCT combined with coronary SSF technology is adequate for TRO CTA imaging in patients with ACP and provides an important CT imaging diagnostic basis for clinical practice.

According to expert consensus [38], the conventional volumes of iodinated CM and saline for pulmonary artery, coronary artery,

Table 7
Comparison of qualitative analysis scores of patients in groups 1-4.

Qualitative Analysis Scores	Group 1 n (%)	K value	Group 2 n (%)	K value	Group 3 n (%)	K value	Group 4 n (%)	K value	Value of test	*P* value
PT										
5	43 (93.5)	0.65	73 (93.6)	0.79					-0.02^{Z}	0.98
4	3 (6.5)		4 (6.4)							
LPT										
5	132 (95.7)	0.65	231 (98.7)	0.66					-1.86^{Z}	0.06
4	6 (4.3)		3 (1.3)							
PRT										
5	151 (82.1)	0.74	274 (87.8)	0.94					-1.77^{Z}	0.08
4	33 (17.9)		38 (12.2)							
LMA										
5	43 (93.5)	0.65			41 (89.1)	0.78			-0.74^{Z}	0.46
4	3 (6.5)				5 (10.9)					
LAD										
5	205 (89.1)	0.69			209 (90.9)	0.69			-0.55^{Z}	0.59
4	22 (9.6)				14 (6.1)					
3	3 (1.3)				7 (3.0)					
LCX										
5	195 (87.1)	0.80			211 (91.7)	0.83			-1.46^{Z}	0.14
4	29 (12.9)				11 (4.8)					
3					8 (1.8)					
RCA										
5	193 (85.0)	0.75			196 (86.0)	0.70			-0.30^{Z}	0.76
4	31 (13.7)				30 (13.2)					
3	3 (1.3)				2 (1.1)					
Aorta										
5	496 (98.0)	0.80					551 (96.3)	0.85	-1.67^{Z}	0.10
4	10 (2.0)						21 (3.7)			
Overall quality										
5	51 (55.4)	0.81	73 (46.8)	0.88	45 (48.9)	0.88	51 (49.0)	0.87	-3.51^{J}	0.60
4	33 (35.9)		77 (49.4)		45 (48.9)		45 (43.3)			
3	8 (8.7)		3 (3.8)		2 (2.2)		8 (7.7)			
Noise										
4	33 (71.7)	0.83	70 (89.7)	0.72	43 (93.5)	0.65	40 (76.9)	0.79	0.66^{J}	0.51
3	13 (28.3)		8 (10.3)		3 (6.5)		12 (23.1)			

Note.—Values are n(%); n: the number of evaluated vascular segments in each group corresponding to the score; %: the percentage of n in the total number of vascular segments in each group.;^{Z}: Z value of Mann-Whitney *U* test; ^{J}: J value of Jonckheere-Terpstra test; PT: Pulmonary Artery Trunk; LPT: Left Pulmonary Artery Trunk; RPT: Right Pulmonary Artery Trunk; LMA: Left Main Coronary Artery; LAD: Left Anterior Descending Artery; LCX: Left Circumflex Artery; RCA: Right Coronary Artery; *: Compared with group 1, $p < 0.05$.

Table 8
Comparison of radiation doses to patients in groups 1-4.

Radiation Dose (units)	Phase of Scanning	Group 1	Group 2	Group 3	Group 4	T value	*P* value
CTDIvol (mGy)	PA	7.81 ± 3.16	7.61 ± 1.93			0.31	0.76
	Coronary	34.00 ± 16.83		41.49 ± 17.86		−1.46	0.15
	Aorta	7.82 ± 2.48			7.96 ± 2.11	−0.2	0.84
DLP (mGy* cm)	PA	285.55 ± 127.81	285.55 ± 127.81			1.09	0.28
	Coronary	619.65 ± 285.56		706.43 ± 254.87		−1.09	0.28
	Aorta	569.07 ± 233.67			551.22 ± 187.22	0.3	0.77
ED (mSv)	PA	4.00 ± 1.79	3.61 ± 1.03			1.09	0.28
	Coronary	16.11 ± 7.42		18.37 ± 6.62		−1.09	0.28
	Aorta	8.25 ± 3.39			7.99 ± 2.71	0.63	0.77

Note.—Values are means ± standard deviations; CTDIvol: CT Dose Index Volume; DLP: Dose Length Product; ED: Effective Dose; PA: Pulmonary Artery; *: Compared with group 1, $p<0.05$.

and aorta CTA scans are approximately 60 + 40 mL, 67 + 45 mL, and 100 + 40 mL, respectively. In the traditional multi-scan protocol, the total volume of iodinated CM and saline used is 227 + 125 mL, leading to a heavy metabolic load on the patient and requiring at least 2–3 days to complete. In this study, the total CM volume was reduced to 66 mL with 38 mL of normal saline in the Group 1, representing a 70.92 % reduction in the total iodine CM usage compared to conventional protocols. The recent Burris et al.'s [39] and Takx RAP et al.'s [40] study used a total volume of 80 mL and 120 mL of iodine CM in the TRO scanning protocol, while our protocol was only 66 mL and achieved good results. This significantly decreases the burden on patients' cardiovascular and renal systems, minimizes CM-related side effects and potential risks, reduces costs, and shortens examination times.

One of the major advantages of TRO CTA scanning is the reduction in diagnosis time for patients. The traditional CTA scanning

method involves separate scans of the pulmonary artery, coronary artery, and aorta, which not only delays the optimal diagnosis and treatment time but also increases the total iodine CM dosage, heightening the risk of adverse reactions [41]. Van Assen et al. reported that the diagnostic efficiency of high CT tube rotation speed is significantly higher than that of low CT tube rotation speed [42]. Faster tube rotation improves temporal resolution, reduces myocardial motion artifacts, and broadens the range of patient heart rates that can be effectively imaged [16,43,44]. Wide-detector CT and dual-source CT achieve high temporal resolution due to their advanced structural properties and superior post-processing systems and software [45–47]. However, their high costs limit their widespread

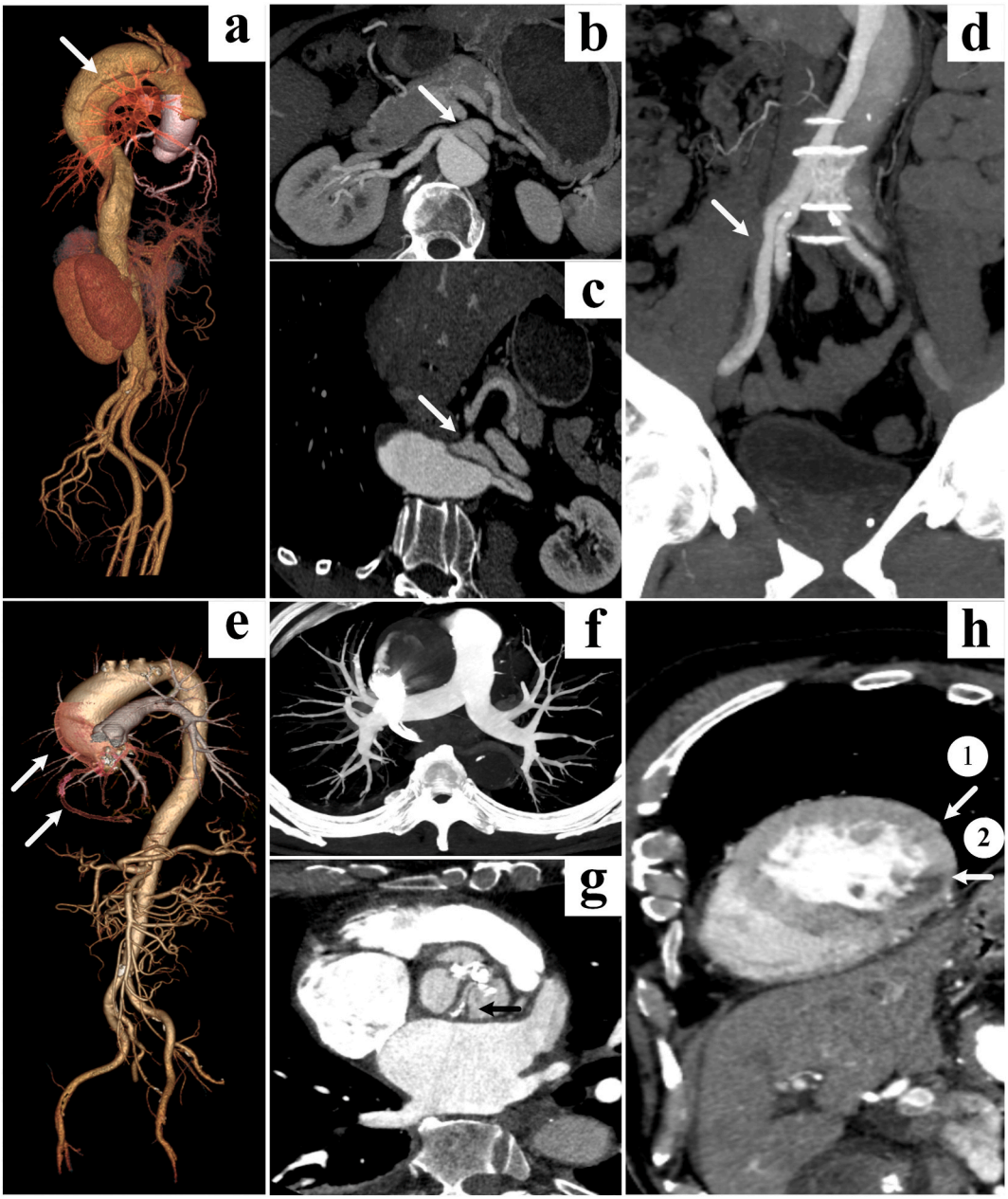

Fig. 5. Case Studies Using Triple-Rule-Out CT Angiography (TRO CTA)
a-d: A 75-year-old male with Stanford type B dissecting aneurysm (indicated by arrows). The right renal artery originates from the false lumen, the left renal artery arises from both the true and false lumens, and there is thrombosis in the false lumen of the right iliac artery. **e-g:** A 66-year-old male with an ascending aortic aneurysm. Post-RCA stent implantation images show almost the maximum intensity projection image of the pulmonary artery without pulmonary vein and precava enhancement interference. There is aortic valve thickening and calcification (indicated by arrows), and decreased myocardial perfusion in the inferior wall of the left ventricle (① CT value 164.18 ± 7.1 vs ② CT value 59.87 ± 14.03), suggesting the possibility of myocardial infarction in the inferior wall of the left ventricle (indicated by arrows). **a** and **e**: Volume rendering (VR) images. **b, c, d, g,** and **h**: Multiplanar reconstruction (MPR) images. **f**: Transverse maximum intensity projection (MIP) image。 .

adoption in primary hospitals and smaller cities, which is not conducive to the timely diagnosis and treatment of acute chest pain. Currently, only 29.45 % of CT devices in China have detector widths of 64 rows or greater [15]. Therefore, it is particularly important to explore whether 64-channel CT combined with coronary SSF technology can provide an important CT imaging diagnostic basis for clinical practice through TRO CTA scanning and whether it is suitable for patients with ACP (Fig. 5).

4.2. Application of injection test with small dose CM in TRO CTA

In this study, there was no significant difference in resting HR between the Group 1 and the control group at the time of examination. Although simple pulmonary artery and aortic CTA imaging typically does not require strict HR control [38,48], Zhang et al. [49] found an inverse relationship between the start delay time of CT scans and the HR of patients. Li Jian et al. [50] found that under the same contrast injection parameters, the cardiac output of the high HR group was higher than that of the low HR group, but the aortic enhanced CT value and delay time of the high HR group were lower than those of the low HR group. To mitigate the potential impact of HR on CT image quality, patients with higher heart rates were administered metoprolol. Consequently, the resting heart rates across all groups were well-controlled (67.55 ± 11.34 BPM), with no significant intergroup differences.

Automatic threshold-trigger scanning and low-dose bolus tests are common pulmonary CTA methods [51,52]. However, studies have shown that automatic threshold triggering alone can result in low pulmonary artery CT values, and prolonged CM injection can

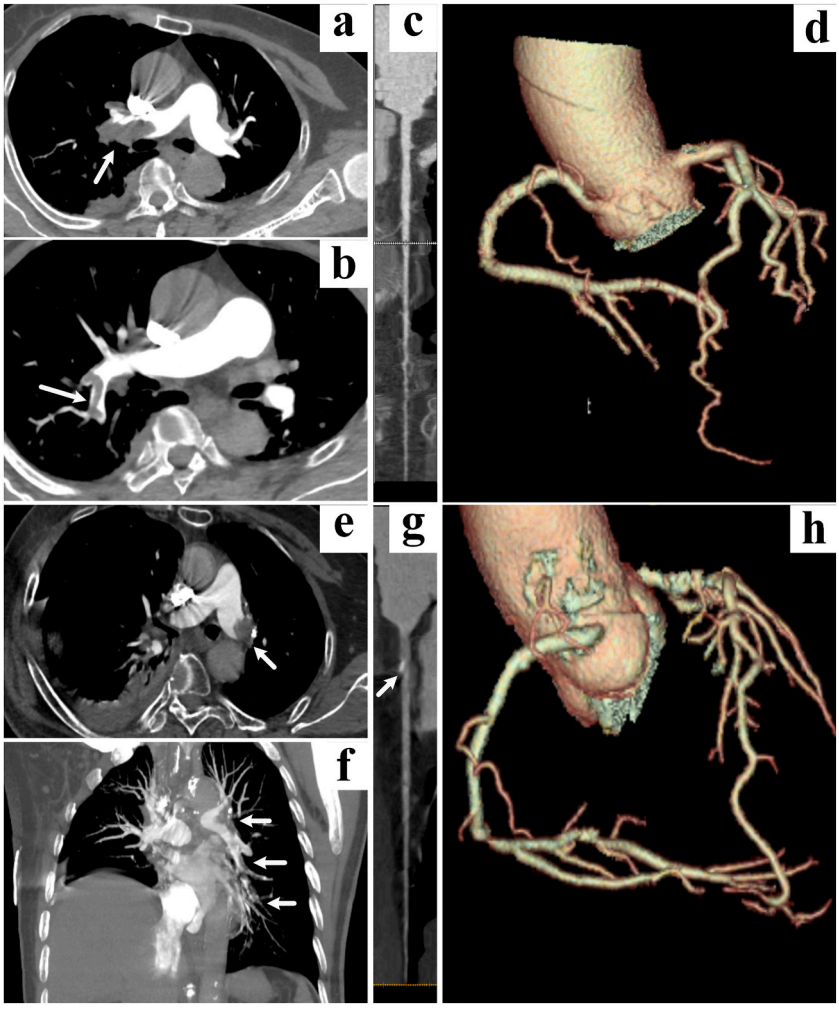

Fig. 6. Case Studies of Pulmonary and Coronary Artery Pathologies Using Triple-Rule-Out CT Angiography (TRO CTA)
a-d: A 63-year-old female, TRO CTA showed multiple pulmonary emboli in the right main pulmonary artery and its branches (indicated by arrows), demonstrating excellent visualization of the coronary vascular tree. **e-f:** A 68-year-old male with multiple pulmonary emboli in the left pulmonary artery (LPA) (indicated by arrows). **g-h:** A 75-year-old male with mixed plaque in the proximal segment of the left anterior descending artery (LAD) causing moderate stenosis (indicated by an arrow), and atherosclerosis in the ascending aorta (indicated by arrows). **d** and **h**: Volume rendering (VR) images. **a, b,** and **e:** Multiplanar reconstruction (MPR) images. **f:** Coronal maximum intensity projection (MIP) image. **c** and **g**: Curved planar reformation (CPR) images.

cause excessive artifacts in the superior vena cava, complicating the capture of pure pulmonary artery phases [53]. The low-dose bolus injection method objectively measures peak CM times, providing accurate scanning windows for pulmonary artery, coronary artery, and thoracoabdominal aorta CTA, thereby ensuring high-quality images and successful pulmonary artery CTA [23].

The low-dose injection method used in this study accurately calculated the peak CM arrival times in the pulmonary artery and aorta, optimizing the start delay time for CT scans and minimizing imaging discrepancies due to varying heart rates. The three-phase injection protocol—rapid iodinated contrast injection, followed by a slow saline-contrast mixture, and a final saline injection—prolongs enhancement duration without increasing CM volume, reduces beam hardening and vorticity artifacts [54], and ensures high-quality pulmonary artery CTA images (Fig. 6a-b, e-f).

4.3. Application of coronary SSF technique

There was no significant difference in the quantitative and qualitative evaluation of coronary CTA images between groups 1 and 3, likely due to well-controlled resting heart rates and the use of coronary SSF technology in both groups. However, emergency patients with high heart rates or arrhythmias pose challenges for traditional 64-channel CT coronary angiography due to insufficient temporal resolution [55]. Faster gantry rotation speeds improve temporal resolution, but further reductions are limited by mechanical constraints and increased costs.

The main reason is the insufficient temporal resolution of conventional 64-channel CT. If the patient's HR is high, the direction and velocity of coronary artery motion will constantly change during the cardiac cycle, which will lead to the failure of image reconstruction centers to coincide, and then lead to stratification, interruption and discontinuity of coronary artery reconstruction images. Star artifacts or layering artifacts, namely blur, ghosting, and trailing artifacts, appear in the image. Increasing the gantry speed is the most direct and effective way to improve the temporal resolution, the faster the gantry rotation, the higher the temporal resolution obtained, and the latest dual-source CT has a gantry rotation time of 0.25s, resulting in high temporal resolution [56].

Half-integral reconstruction involves rotating the X-ray tube 180° plus the scanning angle of the CT detector assembly to obtain the scan data required for reconstruction. This method improves time resolution, but the resolution here refers to "single-sector time resolution." Mahesh et al. [57] demonstrated that for cardiac CTA with an average HR < 60 BPM, the required time resolution is about 250 ms, necessitating a gantry rotation speed of <0.5 s per rotation (s/r). For heart rates of 70–90 BPM, the required time resolution is about 150 ms, requiring a gantry speed of <0.3 s/r. For heart rates >90 BPM, the required temporal resolution is about 100 ms, necessitating a gantry speed of <0.2 s/r. However, increasing gantry rotation speed significantly raises centrifugal forces on the gantry structure, making it challenging to achieve further reductions in gantry rotation time and temporal resolution due to mechanical and manufacturing constraints, as well as increased costs [14].

Recent advancements in software algorithms have improved temporal resolution and reduced motion artifacts [58,59]. Intelligent coronary SSF technology, equipped with GE's third-generation CT machines, enhances image quality by correcting vascular motion artifacts [18]. Studies have shown that SSF technology effectively improves image quality, even in patients with high heart rates or arrhythmias, through the use of ECG editing and intelligent boundary registration. Ma et al. [60] demonstrated higher image quality scores for coronary artery reconstruction images using the SSF technique at 45 % and 75 % phases compared to single-sector and double-sector reconstruction images. Duan et al. [61] and Song et al. [62] showed that for patients with high heart rates or arrhythmias, high-quality images could still be obtained with the SSF algorithm when combined with ECG editing and intelligent boundary registration, optimizing image reconstruction by 6.68 %. Yang et al. [63] found that common factors affecting multi-sector reconstruction had relatively little influence on image reconstruction with the SSF algorithm. Liang et al. [64] showed that SSF technology had better correction effects for subjects with higher but stable heart rates. Wang et al. [65] found that for patients with low and uniform heart rates, there was no significant difference in image quality between the SSF algorithm and the standard algorithm, although the SSF algorithm improved detail display.

Therefore, HR remains the primary factor affecting coronary artery image quality. TRO patients are generally emergency cases requiring rapid CT scans, and their heart rates are often not well controlled. Overall, TRO CTA combined with SSF technology can significantly enhance the success rate and image quality of 64-channel MSCT coronary artery CTA scans (Fig. 6c-d, g-h).

4.4. CT high-pitch scanning technology

In this study, the scanning speed of the Group 1 with high-pitch (pitch = 1.531:1) was 10.19 % higher than that of the control group with conventional pitch (pitch = 1.375:1). Comparison of results showed no significant difference between qualitative and quantitative evaluations, indicating no significant difference in overall image quality. This conclusion is consistent with findings by Wang et al. [66] The author believes that the Group 1's use of high-pitch scanning did not result in decreased image quality, likely due to the noise index, intelligent mA control, and ASiR reconstruction technology used.

The noise index value directly influences image noise and mA. Higher noise index values result in higher image noise and lower mA when KV is constant, and vice versa. Intelligent mA control automatically calculates the required tube current based on the subject's body type and preset image quality parameters (tube voltage, reference current range, and noise index), ensuring consistent X-ray noise across CT images and optimizing the scanning dose. The ASiR reconstruction algorithm, a multi-model image reconstruction algorithm, effectively reduces image noise by selectively identifying and reducing systematic noise and artifacts in the original data space, improving image quality. In this study, ASiR was set to 70 %, effectively reducing image noise and improving the signal-to-noise ratio. Additionally, high-pitch scanning provides faster scanning speeds, improved temporal resolution, and reduced single scanning time and patient breath-holding time, further improving the success rate of emergency chest pain evaluations.

4.5. Radiation dose

The effective radiation dose for pulmonary artery, coronary artery, and aorta CTA in the Group 1 was 28.36 ± 12.6 mSv, slightly lower than the control group's 29.97 ± 10.36 mSv but higher than the 5.65 ± 1.37 mSv reported by Chen et al. [11] using wide-detector prospective axial scanning. Takx RAP et al. showed that the ED was 20.7 ± 10.7 mSv under the 120 KV TRO CTA scanning condition with the scanning range only including the thorax [40]. One reason for this difference is that the tube voltage in their study was 100 kV, whereas this study used the guideline-recommended 120 kV to ensure examination success and avoid missing atypical lesions [38,67]. Murphy et al. [52] suggested that calcified atherosclerotic plaques or metallic stents can be exaggerated at low kV, complicating CTA interpretation. Additionally, the conversion coefficient k value used in Chen et al.'s study was 0.014 mSv/(mGy * cm) [11] and Takx RAP et al.'s study was 0.017 mSv/(mGy * cm) [40], whereas this study used the latest conversion coefficient of 0.026 mSv/(mGy * cm) for cardiac CT scanning [35,36]. Furthermore, the radiation dose for aortic CTA was calculated for the entire scanning area (thoracic inlet to the lower end of the pubic symphysis), not just the area from the thoracic inlet to the upper edge of the diaphragm.

Malaisrie SC et al. [68] reported that tissue and organ malperfusion is a life-threatening complication of aortic dissection. The occurrence of peripheral tissue and organ malperfusion can lead to ischemia of the tissue and organ vascular bed, resulting in malperfusion syndrome characterized by end-organ dysfunction. It can be manifested as a series of clinical features of varying severity, from systemic inflammatory response, metabolic disorders to obvious organ infarction. For example, aortic dissection combined with mesenteric malperfusion is fatal, and the mortality rate of proximal aortic repair in such patients is as high as 41–100 %. The diagnosis

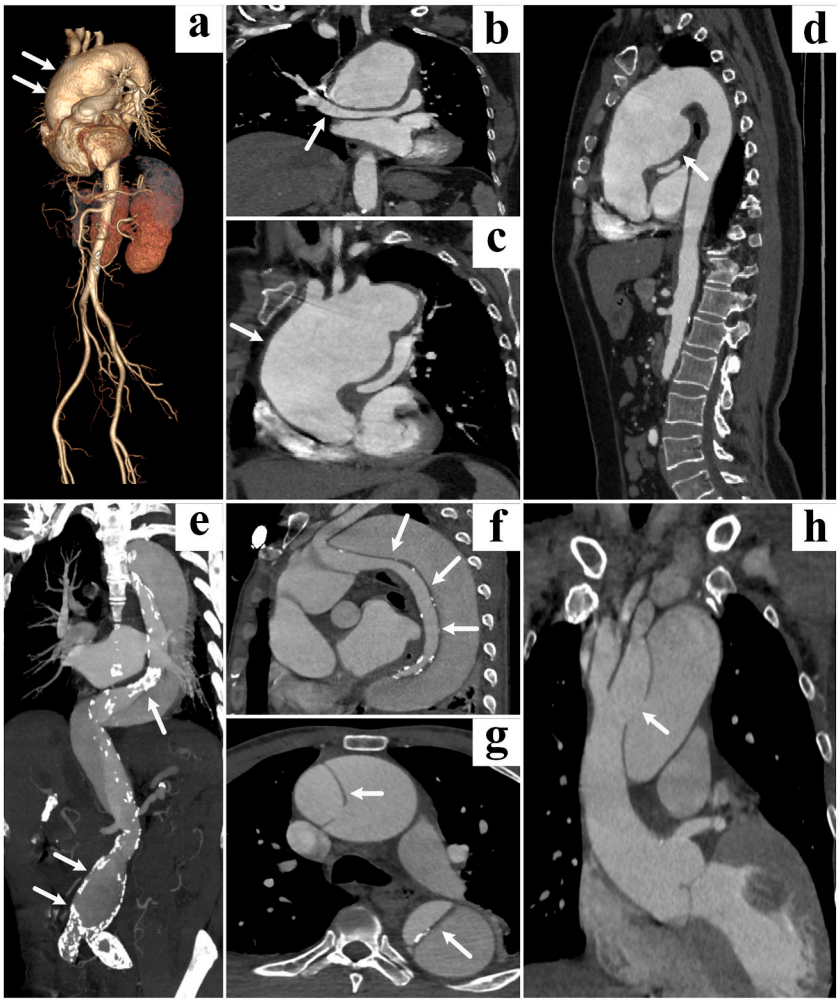

Fig. 7. Case Studies of Aortic Pathologies Using CT Angiography (CTA)
a-d: A 43-year-old female with an ascending aortic aneurysm (indicated by arrows) and pulmonary artery compression (indicated by arrows). **e-h:** A 49-year-old male with DeBakey type I and Stanford type A aortic dissection, lower abdominal aorta and bilateral common iliac artery aneurysms, and aortic atherosclerosis (indicated by arrows). **a:** Volume rendering (VR) image. **b-d** and **f-h:** Multiplanar reconstruction (MPR) images. **e:** Coronary maximum intensity projection (MIP) image.

of malperfusion syndrome is also difficult, but due to the compression of the true lumen of the abdominal aortic segment, mesenteric malperfusion is usually associated with malperfusion of the liver, kidney, and iliac femoral artery. Multi-center studies have shown that mortality is positively correlated with the number of vascular beds affected. Delayed diagnosis usually leads to reduced blood supply time to organs, irreversible microvascular spasm, and transmural intestinal infarction at the time of eventual reperfusion. To improve the prognosis of such high-risk patients, it is necessary to quickly diagnose and reverse their ischemic condition, while minimizing the risk of aortic rupture. An example of this is the case in which the renal artery was found to arise from the false lumen (Fig. 5). In this figure, we illustrate the diagnostic capabilities of TRO CTA combined with the coronary Snap-Shot Freeze technique in acute chest pain evaluation. The images provide detailed visualization of complex vascular pathologies, such as dissecting aneurysms and post-stent implantation changes, along with myocardial perfusion assessments. These case studies underscore the precision and comprehensive nature of this advanced imaging modality, enhancing its clinical utility in diagnosing and managing acute chest pain. Therefore, scanning the whole range of the aorta is helpful to diagnose whether the patient has the possibility of peripheral tissue and organ malperfusion, and help to make timely surgical or drug treatment plans, so as to maximize the benefits of patients (Fig. 7).

The absence of a statistically significant difference in radiation dose between Group 1 and the control group can be attributed to several technical and procedural factors. The CTDIvol is calculated as the ratio of CTDIw to pitch [69]. In Group 1, a higher pitch (1.531:1 compared to 1.375:1) and increased CT tube rotation speed (0.4 s versus 0.5 s) were utilized to enhance temporal resolution and scanning efficiency. When KV is constant, although the synergistic effects of ASiR, noise index, Auto mA, and Smart mA control may slightly increase mA to achieve comparable image quality [70], resulting in a corresponding increase in CTDIw, the higher pitch in Group 1 stabilizes the CTDIvol. Additionally, demographic similarities between the groups, including BMI and scanned areas, resulted in comparable DLP and ED values, ensuring consistent radiation exposure across patient groups. This confirms that 64-channel MSCT combined with SSF technology delivers noninferior quality imaging with consistent radiation doses, ensuring patient safety.

4.6. Limitations and prospects

This study's limitations include a relatively small sample size, a limited number of patients with severe obesity, high heart rates, high calcium burden or arrhythmias, and the lack of a multicenter study and comparative analysis with multiple CT devices. Future research should explore and optimize scanning protocols, contrast injection protocols, and trigger protocols to further reduce radiation doses and CM volumes.

In conclusion, 64-channel MSCT combined with intelligent coronary SSF technology enables comprehensive CT imaging of the pulmonary artery, coronary artery, aorta, and thoracoabdominal tissues and organs. Advanced software algorithms correct image artifacts and optimize images without altering the operational process, reducing the number of CT scans required and ensuring high image quality. This study provides a theoretical basis for TRO CTA using non-wide-detector, non-dual-energy, and non-spectral CT, reducing iodine CM dosage, maintaining patient radiation doses, providing timely and accurate diagnostic information, and improving emergency patient outcomes. The reliability and accuracy of these findings support their clinical application.

CRediT authorship contribution statement

Jie Feng: Writing – original draft. **Jiale Zeng:** Writing – review & editing, Formal analysis. **Qiye Xu:** Data curation. **Jiatian Lu:** Data curation. **Yanru Pei:** Formal analysis, Data curation. **Xiang Zhang:** Writing – review & editing, Validation, Supervision. **Ming Gao:** Writing – review & editing, Validation, Supervision, Conceptualization.

Informed consent

Written informed consent was obtained from all subjects (patients) in this study.

Guarantor

The scientific guarantor of this publication is Ming Gao.

Consent for publication

All the authors of this manuscript have read and approved its publication.

Ethical approval

Institutional Review Board approval was obtained.

Funding

This study was supported by Medical Science and Technology Foundation of Guangdong Province (2022111523109847).

Key Points

- High-Quality Imaging: 64-channel MSCT with SSF technique produces noninferior high-quality TRO CTA images comparable to traditional methods.
- Reduced Contrast Medium Usage: The combined approach significantly reduces the total injection volume of iodine CM by 70.92 % compared to conventional multiple scans protocols, decreasing the metabolic load on patients.
- Consistent Radiation Dose: Radiation doses are maintained at consistent levels across different patient groups, ensuring patient safety.
- Enhanced Diagnostic Efficiency: The technique allows for comprehensive imaging of the pulmonary artery, coronary artery, and aorta in a single scan, improving diagnostic efficiency and reducing examination time.

Declaration of competing interest

The authors declare that they have no known competing financial interests or personal relationships that could have appeared to influence the work reported in this paper.

Acknowledgements

Not Applicable.

References

[1] Report on cardiovascular health and diseases in China 2021: an updated summary, Biomed. Environ. Sci. 35 (7) (2022) 573–603.
[2] N. Pattereth, et al., The role of triple rule-out CT in an Indian emergency setting, Indian J. Crit. Care Med. 27 (3) (2023) 190–194.
[3] M.K. Chae, et al., Triple rule-out computed tomography for risk stratification of patients with acute chest pain, J Cardiovasc Comput Tomogr 10 (4) (2016) 291–300.
[4] M.P. Monica, et al., Computed tomographic angiography for risk stratification in patients with acute chest pain - the triple rule-out concept in the emergency department, Curr Med Imaging Rev 16 (2) (2020) 98–110.
[5] China Alliance of Chest Pain Centers, et al., Summary of quality control report of Chinese chest pain center (2021), Chin. J. Interventional Cardiol. 30 (5) (2022) 321–327 (in Chinese).
[6] O. Shi, et al., Factors associated with door-in to door-out delays among ST-segment elevation myocardial infarction (STEMI) patients transferred for primary percutaneous coronary intervention: a population-based cohort study in Ontario, Canada, BMC Cardiovasc. Disord. 18 (1) (2018) 204.
[7] K.M. Takakuwa, E.J. Halpern, Evaluation of a "triple rule-out" coronary CT angiography protocol: use of 64-Section CT in low-to-moderate risk emergency department patients suspected of having acute coronary syndrome, Radiology 248 (2) (2008) 438–446.
[8] E. Marijon, et al., The Lancet Commission to reduce the global burden of sudden cardiac death: a call for multidisciplinary action, Lancet 402 (10405) (2023) 883–936.
[9] S.S. Martin, et al., Value of machine learning-based coronary CT fractional flow reserve applied to triple-rule-out CT angiography in acute chest pain, Radiol Cardiothorac Imaging 2 (3) (2020) e190137.
[10] K. Perisinakis, et al., Triple-rule-out computed tomography angiography with 256-slice computed tomography scanners: patient-specific assessment of radiation burden and associated cancer risk, Invest. Radiol. 47 (2) (2012) 109–115.
[11] Y. Chen, et al., Triple-rule-out CT angiography using two axial scans with 16 cm wide-detector for radiation dose reduction, Eur. Radiol. 28 (11) (2018) 4654–4661.
[12] Lianzhi Tang, et al., Dual source CT high pitch prospective scan in triple-rule-out acute chest pain examination, Chinese Journal of Medical Imaging (3) (2015) 200–203, 208(in Chinese).
[13] A.M. Wnorowski, E.J. Halpern, Diagnostic yield of triple-rule-out CT in an emergency setting, AJR Am. J. Roentgenol. 207 (2) (2016) 295–301.
[14] T.G. Flohr, R. Raupach, H. Bruder, Cardiac CT: how much can temporal resolution, spatial resolution, and volume coverage be improved? J Cardiovasc Comput Tomogr 3 (3) (2009) 143–152.
[15] Lv. Bin, et al., Survey of the application status of cardiovascular imaging modalities and medical quality report in China, Chinese Circ. J 35 (7) (2020) 625–633 (in Chinese).
[16] Y.J. Choi, et al., Cardiac cine CT approaching 1 mSv: implementation and assessment of a 58-ms temporal resolution protocol, Int J Cardiovasc Imaging 36 (8) (2020) 1583–1591.
[17] Y. Chen, et al., Chinese expert consensus on adverse reactions related to the application of iodinated contrast media angiography, Chinese J Interventional Cardiology (6) (2014) 341–348 (in Chinese).
[18] Q. Li, et al., Effect of a novel motion correction algorithm (SSF) on the image quality of coronary CTA with intermediate heart rates: segment-based and vessel-based analyses, Eur. J. Radiol. 83 (11) (2014) 2024–2032.
[19] A. Sabarudin, Z. Sun, Beta-blocker administration protocol for prospectively ECG-triggered coronary CT angiography, World J. Cardiol. 5 (12) (2013) 453–458.
[20] R.A. Takx, et al., Sublingual nitroglycerin administration in coronary computed tomography angiography: a systematic review, Eur. Radiol. 25 (12) (2015) 3536–3542.
[21] X. Ming, M. Wang, The dosimetric difference in IMRT treatment planning based on different isocenter positions for the thoracic and abdominal large target volume, Journal of Radiation Research and Radiation Technology 32 (4) (2014) 21–26 (in Chinese).
[22] Q. Gu, et al., Study on the feasibility of ultra-low dose contrast agent bolus injection during pulmonary artery angiography by computer tomography, J. Med. Imag. 29 (5) (2019) 753–756 (in Chinese).
[23] H. Wu, et al., An optimized test bolus for computed tomography pulmonary angiography and its application at 80 kV with 10 ml contrast agent, Sci. Rep. 10 (1) (2020) 10208.
[24] Z. Zhang, Magnetic resonance image features and their mechanism of contrast (I): signal, noise and signal-to-noise ratio, Diagnostic imaging and interventional radiology 26 (4) (2017) 344–347 (in Chinese).
[25] Z. Zhang, Magnetic resonance image characteristics and its contrast mechanism (II): image contrast and contrast-to-noise ratio, Diagnostic imaging and interventional radiology 26 (5) (2017) 430–433 (in Chinese).

[26] W.G. Austen, et al., A reporting system on patients evaluated for coronary artery disease. Report of the ad hoc committee for grading of coronary artery disease, council on cardiovascular surgery, American heart association, Circulation 51 (4 Suppl) (1975) 5–40.
[27] H. Murillo, et al., Imaging of the aorta: embryology and anatomy, Semin. Ultrasound CT MR 33 (3) (2012) 169–190.
[28] M.L. Gunn, Imaging of aortic and branch vessel trauma, Radiol Clin North Am 50 (1) (2012) 85–103.
[29] J. Paul, et al., Image fusion in dual energy computed tomography for detection of various anatomic structures–effect on contrast enhancement, contrast-to-noise ratio, signal-to-noise ratio and image quality, Eur. J. Radiol. 80 (2) (2011) 612–619.
[30] G. De Rubeis, et al., Pilot study of the multicentre DISCHARGE Trial: image quality and protocol adherence results of computed tomography and invasive coronary angiography, Eur. Radiol. 30 (4) (2020) 1997–2009.
[31] G. Bongartz, S.J. Golding, A.G. Jurik, e.a, European guidelines for multislice computed tomography: appendix A, in: European Guidelines for Multislice Computed Tomography Funded by the European Commission, 2004.
[32] H. Murillo, et al., Pulmonary circulation imaging: embryology and normal anatomy, Semin. Ultrasound CT MR 33 (6) (2012) 473–484.
[33] H. Liu, Study on the Estimation Model of Patient Dose from Diagnostic X-Ray Examination, Fudan University, 2009 (in Chinese).
[34] J.J. DeMarco, et al., Estimating radiation doses from multidetector CT using Monte Carlo simulations: effects of different size voxelized patient models on magnitudes of organ and effective dose, Phys. Med. Biol. 52 (9) (2007) 2583–2597.
[35] W. Huda, et al., Computing effective dose in cardiac CT, Phys. Med. Biol. 55 (13) (2010) 3675–3684.
[36] S. Trattner, et al., Cardiac-specific conversion factors to estimate radiation effective dose from dose-length product in computed tomography, JACC Cardiovasc Imaging 11 (1) (2018) 64–74.
[37] China State Administration for Market Regulation, S.A.o.C., Methods for estimating organ doses to examined patients in diagnostic X-ray, GB/T 16137-2021(in Chinese), 2021.
[38] Chinese Society Radiology, Expert consensus on CT examination technology, Chinese Radiol. J. 50 (12) (2016) 916–928 (in Chinese).
[39] A.C. Burris 2nd, et al., Triple rule out versus coronary CT angiography in patients with acute chest pain: results from the ACIC consortium, JACC Cardiovasc Imaging 8 (7) (2015) 817–825.
[40] R.A.P. Takx, et al., Low-tube-voltage selection for triple-rule-out CTA: relation to patient size, Eur. Radiol. 27 (6) (2017) 2292–2297.
[41] R.D.N. Group, P.C.o.R.N. Care, R.B.o.C.M. Association, Expert consensus on the safety of iodine contrast agent infusion in imaging department, Journal of Interventional Radiology 27 (8) (2018) 707–712 (in Chinese).
[42] M. van Assen, et al., Low CT temporal sampling rates result in a substantial underestimation of myocardial blood flow measurements, Int J Cardiovasc Imaging 35 (3) (2019) 539–547.
[43] T.G. Flohr, et al., Dual-source spiral CT with pitch up to 3.2 and 75 ms temporal resolution: image reconstruction and assessment of image quality, Med. Phys. 36 (12) (2009) 5641–5653.
[44] N. Akino, et al., [Evaluation of time resolution in cardiac synchronized image reconstruction using multi-slice CT], Nihon Hoshasen Gijutsu Gakkai Zasshi 61 (3) (2005) 409–418.
[45] K. Matsubara, et al., Contrast resolution in multidetector-row CT with 16 detector rows: phantom study, Radiol. Phys. Technol. 1 (1) (2008) 13–19.
[46] N. Çullu, et al., Evaluation of the morphological and clinical features of left anterior descending myocardial bridging with multi-detector computed tomography, Kardiochir Torakochirurgia Pol 18 (2) (2021) 87–91.
[47] B. Schmidt, T. Flohr, Principles and applications of dual source CT, Phys. Med. 79 (2020) 36–46.
[48] W. Zhang, P. Liu, Analysis of the correlation between heart rate fluctuations and the image quality and radiation dose of patients with one-stop head and neck cardiovascular CTA scan, Imaging Science and Photochemistry 39 (2) (2021) 292–297 (in Chinese).
[49] L. Zhang, To analyze the relationship between the start-up time of 64-channel CT tracking scanning head and neck CTA imaging technology and the heart rate of patients, Imaging research and medical applications 3 (2) (2019) 51–52 (in Chinese).
[50] J. Li, et al., The effect of heart rate on left cardiac function index,enhanced CT value of aorta and delay time, Practice in Radiology (11) (2015) 1111–1113 (in Chinese).
[51] M.H. Albrecht, et al., State-of-the-Art pulmonary CT angiography for acute pulmonary embolism, AJR Am. J. Roentgenol. 208 (3) (2017) 495–504.
[52] D.J. Murphy, A. Aghayev, M.L. Steigner, Vascular CT and MRI: a practical guide to imaging protocols, Insights Imaging 9 (2) (2018) 215–236.
[53] K.T. Bae, Intravenous contrast medium administration and scan timing at CT: considerations and approaches, Radiology 256 (1) (2010) 32–61.
[54] J.M. Schussler, E.R. Smith, Sixty-four-slice computed tomographic coronary angiography: will the "triple rule out" change chest pain evaluation in the ED? Am. J. Emerg. Med. 25 (3) (2007) 367–375.
[55] H. Saito, et al., Characteristics of temporal resolution in 16- and 64-row computed tomography scanners, Radiol. Phys. Technol. 11 (1) (2018) 100–108.
[56] M.M. Ochs, et al., Strengths and limitations of coronary angiography with turbo high-pitch third-generation dual-source CT, Clin. Radiol. 72 (9) (2017) 739–744.
[57] M. Mahesh, D.D. Cody, Physics of cardiac imaging with multiple-row detector CT, Radiographics 27 (5) (2007) 1495–1509.
[58] J. Hahn, et al., Motion compensation in the region of the coronary arteries based on partial angle reconstructions from short-scan CT data, Med. Phys. 44 (11) (2017) 5795–5813.
[59] J. Maier, et al., Deep learning-based coronary artery motion estimation and compensation for short-scan cardiac CT, Med. Phys. 48 (7) (2021) 3559–3571.
[60] H. Ma, Evaluation the Influence of Snapshot Freeze Technique on Image Quality of Coronary CT Angiography:compared with multi.Sector Reconstruction, Xinjiang Medical University, 2015 (in Chinese).
[61] B. Duan, et al., Application value of snap shot freeze combined with intelligent boundary registration in the diagnosis of myocardial bridging with gem energy spectrum CT coronary angiography, J. Med. Imag. 31 (4) (2021) 556–560 (in Chinese).
[62] W. Song, et al., Application value of SSF combined with IBR technique in diagnosing MB by coronary angiography with gem energy spectrum CT, China Medical Equipment 18 (6) (2021) 95–98 (in Chinese).
[63] X. Yang, et al., Motion artifact correction by snapshot freeze in coronary CT angiography at different levels of coronary enhancement, J. Med. Imaging Health Inform. 6 (2) (2016) 551–554.
[64] J. Liang, et al., Impact of SSF on diagnostic performance of coronary computed tomography angiography within 1 heart beat in patients with high heart rate using a 256-row detector computed tomography, J. Comput. Assist. Tomogr. 42 (1) (2018) 54–61.
[65] B. Wang, et al., Application value of coronary artery snapshot freeze technique in improving the image quality of coronary CTA with retrospective ECG-gating technique, Practice in Radiology 32 (4) (2017) 427–430 (in Chinese).
[66] K. Wang, et al., Dedicated ccta followed by high-pitch scanning versus TRO-CT for contrast media and radiation dose reduction: a retrospective study, Diagnostics 12 (11) (2022).
[67] E. Atlı, et al., Radiation doses from head, neck, chest and abdominal CT examinations: an institutional dose report, Diagn Interv Radiol 27 (1) (2021) 147–151.
[68] S.C. Malaisrie, et al., The American Association for Thoracic Surgery expert consensus document: surgical treatment of acute type A aortic dissection, J. Thorac. Cardiovasc. Surg. 162 (3) (2021) 735–758.e2, 2021.
[69] K.D. DePew, et al., Direct measurement of CTDI(w) on helical CT scans, J. Appl. Clin. Med. Phys. 23 (11) (2022) e13761.
[70] K.J. Chang, et al., Optimizing CT technique to reduce radiation dose: effect of changes in kVp, iterative reconstruction, and noise index on dose and noise in a human cadaver, Radiol. Phys. Technol. 10 (2) (2017) 180–188.

Abbreviations

AA_FHH: Abdominal Aorta at the Level of the First Hepatic Hilum
ACP: Acute Chest Pain

ACS: Acute Coronary Syndrome
ASIR: Adaptive Statistical Iterative Reconstruction
AW 4.7: Advanced Workstation 4.7
ANOVA: Analysis of Variance
AAr: Aortic Arch
AD: Aortic Dissection
AR: Aortic Root
AA: Ascending Aorta
AAo: Ascending Aorta Orifice
BPM: Beats Per Minute
BMI: Body Mass Index
CTA: Computed Tomography Angiography
CI: Confidence Intervals
CM: Contrast Medium
CNR: Contrast-to-Noise Ratio
CA: Coronary Artery
CTDIvol: CT Dose Index Volume
CPR: Curved Planar Reconstruction
DAo: Descending Aorta
DW: Door-to-Wire
DLP: Dose Length Product
ED: Effective Dose
ECG: Electrocardiogram
HR: Heart Rates
HU: Hounsfield Unit
ICC: Intraclass Correlation Coefficient
IV: Intravenous
LMA: Left Main Coronary Artery
LVLW: Left Ventricular Lateral Wall
LPT/RPT: Left/Right Pulmonary Artery Trunk
MIP: Maximum Intensity Projection
MPR: Multiplanar Reformation
MSCT: Multi-Slice Computed Tomography
PCI: Percutaneous Coronary Intervention
PF: Pericardial Fat
LAD-p: Proximal Left Anterior Descending Artery
LCX-p: Proximal Left Circumflex Artery
RCA-p: Proximal Right Coronary Artery
PA: Pulmonary Artery
PT: Pulmonary Artery Trunk
PTE: Pulmonary Thromboembolism
ROI: Regions of Interest
RESBT: Right Erector Spinae at the Bifurcation of the Trachea
SNR: Signal-to-Noise Ratio
SSF: Snap-Shoot Freeze
SD: Standard Deviation
STEMI: St-Segment Elevation Myocardial Infarction
SMC: Symptom-to-First Medical Contact
3D: Three-Dimensional
TRO: Triple-Rule-Out
VR: Volume Rendering